PROCEEDINGS OF SCIENCE

Neutrino Astrophysics

Francis Halzen[*†]
University of Wisconsin–Madison, Madison, WI
E-mail: halzen@icecube.wisc.edu

By transforming a cubic kilometer of natural Antarctic ice into a neutrino detector, the IceCube project created the opportunity to observe cosmic neutrinos. We describe the experiment and the complementary methods presently used to study the flux of the recently discovered cosmic neutrinos. In one method, events are selected in which neutrinos interacted inside the instrumented volume of the detector, yielding a sample of events dominated by neutrinos of electron and tau flavor. Alternatively, another method detects secondary muons produced by neutrinos selected for having traveled through the Earth to reach the detector, providing a pure sample of muon neutrinos. We will summarize the results obtained with the enlarged data set collected since the initial discovery and appraise the current status of high-energy neutrino astronomy. Continued observations are closing in on the source candidates. In this context, we highlight the potential of multimessenger analyses as well as the compelling case for constructing a next-generation detector larger by one order of magnitude in volume.

The European Physical Society Conference on High Energy Physics
22–29 July 2015
Vienna, Austria

[*]Speaker.

[†]Discussion with collaborators inside and outside the IceCube Collaboration, too many to be listed, have greatly shaped this presentation. Thanks. This research was supported in part by the U.S. National Science Foundation under Grants No. ANT-0937462 and PHY-1306958 and by the University of Wisconsin Research Committee with funds granted by the Wisconsin Alumni Research Foundation.

PoS(EPS-HEP2015)014

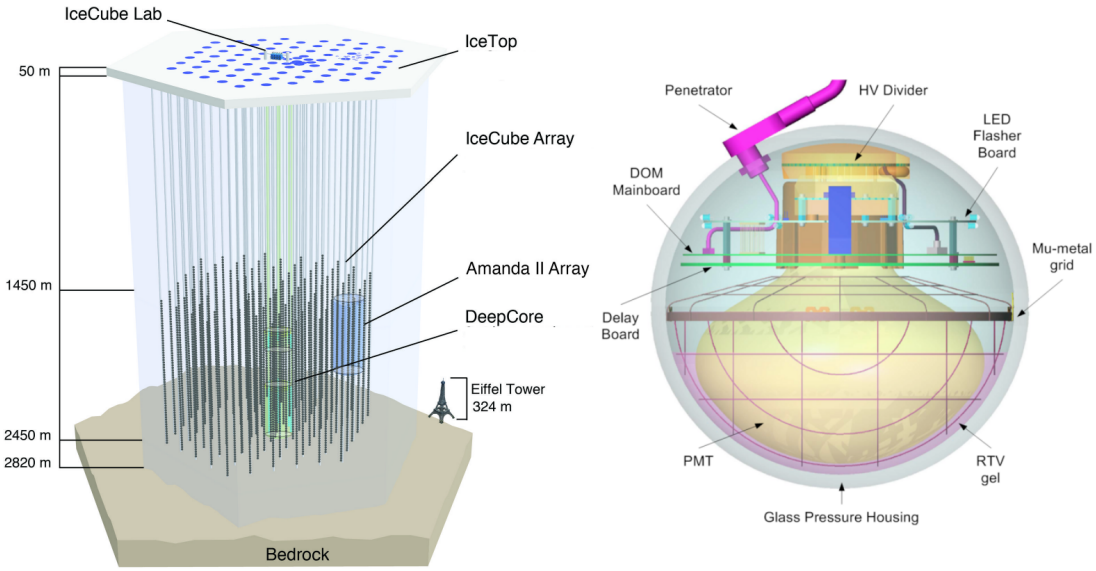

Figure 1: Sketch of the IceCube observatory (left) and the digital optical module, or DOM (right).

1. Introduction

Soon after the 1956 observation of the neutrino [1], the idea emerged that it represented the ideal astronomical messenger [2, 3, 4]. Neutrinos can reach us from the edge of the Universe without absorption and with no deflection by magnetic fields. They can escape unscathed from the inner neighborhood of black holes and from the accelerators where cosmic rays are born. The weak interactions that turn neutrinos into ideal astronomical messengers also make them notoriously difficult to detect. It has been anticipated for some time that kilometer-scale particle detectors are required to collect neutrinos from the cosmos in statistically significant numbers [5, 6, 7, 8]. Already by 1969, it had been understood [9] that such an instrument would create the possibility of observing the so-called Greisen-Zatsepin-Kuzmin (GZK) neutrinos produced in the interactions of cosmic rays with background microwave photons [10].

Given the detector's required size, early efforts concentrated on instrumenting large volumes of natural water with photomultipliers [11] that detect the Cherenkov light emitted by secondary particles produced when neutrinos interact with nuclei inside or near the detector [12, 13, 14, 15, 16, 17]. In contrast, the IceCube detector [18, 19, 20, 21] transforms deep natural Antarctic ice into a Cherenkov detector. The instrument shown in Fig. 1 consists of 86 strings, each instrumented with 60 ten-inch photomultipliers spaced 17 m apart over a total length of one kilometer. The deepest modules are located at a depth of 2.45 km so that the instrument is shielded from the large background of cosmic rays at the surface by approximately 1.5 km of ice. Strings are arranged at apexes of equilateral triangles that are 125 m on a side. The instrumented detector volume is a cubic kilometer of dark and highly transparent [22] Antarctic ice.

Neutrino events may be broadly classified in two groups that reflect the patterns of Cherenkov light emitted, muon tracks and particle showers (often referred to as cascades). Tracks are produced

by charged current interactions of muon neutrinos, while cascades are produced by charged current interactions of electron and tau neutrinos as well as neutral current interactions of all flavors. The travel range of ν_μ-induced muons is on the order of kilometers, while the length characteristic of the electromagnetic showers that dominate the cascade events is only tens of meters.

A detailed understanding of the propagation of photons in the Antarctic ice [22] is essential in order to relate light generated to light observed in the digital optical modules (DOMs) that house and record the signals of the photomultipliers [20]: the arrival time of photons at the DOMs determines the trajectory [23], while the number of photons determine the deposited energy. For typical kilometer-long tracks, the angular resolution is better than 0.4°. Reconstruction of the direction of cascade events is still in the development stage in IceCube [24]. The direction of cascades can be reconstructed to within 15° based on photon timing patterns collected by individual DOMs. Determining the deposited energy from the observed light pool is relatively straightforward, and a resolution of better than 15 % is possible; the same value holds for the reconstruction of the energy deposited by a muon track inside the detector. At this point, IceCube's precision in reconstruction is limited by computing, not by the properties of the Cherenkov medium, guaranteeing improved performance in the future.

Another way to classify neutrino events is to distinguish between events that start inside the detector from those in which the neutrino interacts outside the detector. By specializing to events starting inside the detector, one detects neutrinos of all flavors. For $E_\nu < 1$ PeV, the interaction of a ν_τ in IceCube will look much like that of a ν_e because the track length of the ν_τ of less than 50 m is smaller than the 125 m string spacings and difficult to identify. The largest neutrino sample consists of ν_μ-induced muon tracks entering the detector from zenith angles too large to be atmospheric in origin, typically $\theta \geq 85^\circ$. The muons are secondaries produced by neutrinos that have penetrated the Earth. The rate of such events in the full IceCube detector is approximately 200 per day or more, depending on the threshold for a particular analysis. Their mean energy is $1 \sim 10$ TeV.

For neutrino astronomy, the first challenge is to select sufficiently pure samples of neutrinos, and the second is to identify the small fraction of the neutrinos that are astrophysical in origin, expected to be at most tens of events per year. Atmospheric neutrinos are an overwhelming background for cosmic neutrinos, at least at energies below ~ 100 TeV. Above this energy, however, their flux is too small to produce events in a kilometer-scale detector and every event is a discovery. This is how IceCube made its initial serendipitous observation of cosmic neutrinos.

2. The Status of Neutrino Astronomy

GZK neutrinos were the target of a dedicated search using IceCube data collected between May 2010 and May 2012. Two interesting events were found [25]. However, their energies, rather than EeV as expected for GZK neutrinos, were in the PeV range: 1,040 TeV and 1,140 TeV. The events are particle showers initiated by neutrinos interacting inside the instrumented detector volume. Their light pool of roughly one hundred thousand photoelectrons extends over more than 500 meters; see Fig. 2. With no evidence of a muon track, they are showers initiated by electron or tau neutrinos. With PeV energy, they are unlikely to be atmospheric in origin.

Previous to this serendipitous discovery, neutrino searches had almost exclusively specialized to the observation of muon neutrinos that interact primarily outside the detector to produce

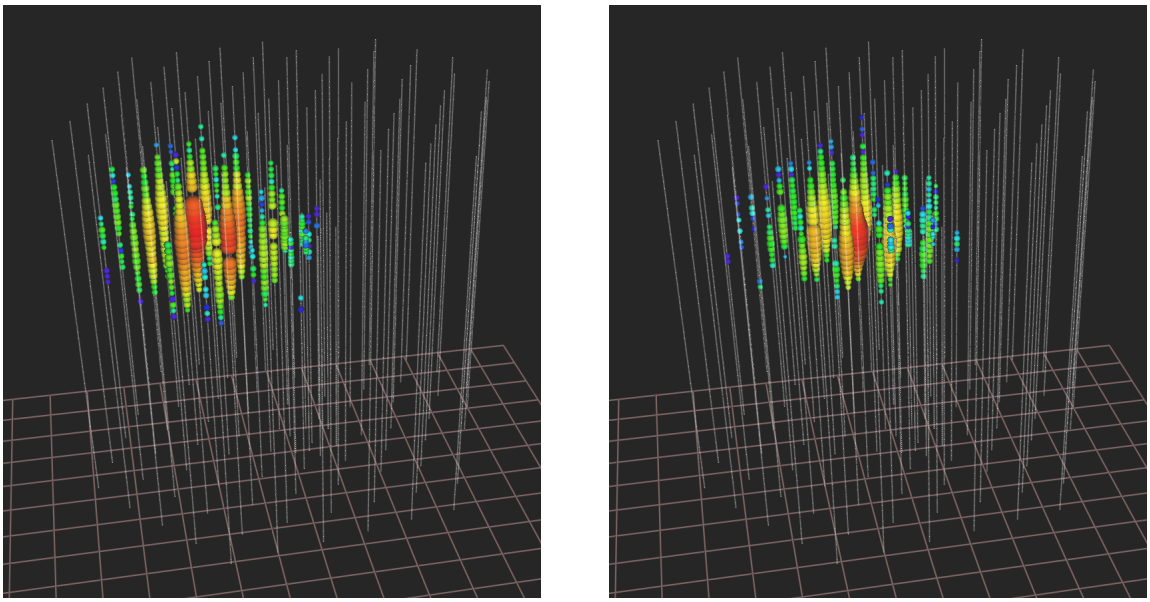

Figure 2: Light pool produced in IceCube by the two cascades "Bert" (left) and "Ernie" (right). Their measured energy is 1.04 PeV and 1.14 PeV, respectively, which represents a lower limit on the energy of the neutrino that initiated each shower. White dots represent sensors with no signal. For the colored dots, color indicates arrival time, from red (early) to purple (late) following the rainbow, and size reflects the number of photons detected.

kilometer-long muon tracks passing through the instrumented volume. Although creating the opportunity to observe neutrinos interacting outside the detector, it is necessary to use the Earth as a filter to remove the huge background flux of muons produced by cosmic ray interactions in the atmosphere. This limits the neutrino view to a single flavor and half the sky. Inspired by the observation of the two PeV events, a filter was designed that exclusively identifies neutrinos interacting inside the detector. It divides the instrumented volume of ice into an outer veto shield and a 420 megaton inner fiducial volume. The separation between veto and signal regions was optimized to reduce the background of atmospheric muons and neutrinos to a handful of events per year while keeping 98% of the signal. The great advantage of specializing to neutrinos interacting inside the instrumented volume of ice is that the detector functions as a total absorption calorimeter measuring energy with a 10-15 % resolution. Also, neutrinos from all directions in the sky can be identified, including both muon tracks produced in ν_μ charged-current interactions and secondary showers produced by neutrinos of all flavors.

Analyzing the data covering the same time period as the GZK neutrino search, 28 candidate neutrino events were identified with in-detector deposited energies between 30 and 1140 TeV; see Fig. 3. Of these, 21 are showers. The remaining seven events are muon tracks, which do allow for subdegree angular reconstruction; only a lower limit on their energy can be established because of the unknown fraction carried away by the exiting muon track. Furthermore, with the present statistics, these are difficult to separate from a remnant of the competing atmospheric muon background. The 28 events include the two PeV events previously revealed in the GZK neutrino search.

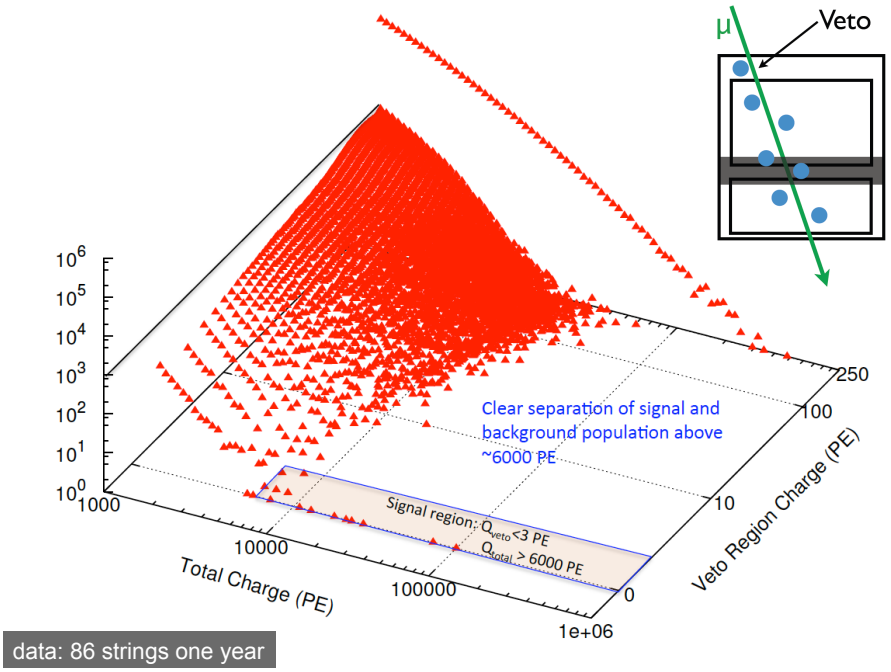

Figure 3: One year of IceCube data from its final 86-string configuration showing number of events as a function of the total number of photoelectrons and the number present in the veto region. The signal region is defined as having more than 6000 photoelectrons with fewer than three of the first 250 in the veto region of the detector. The signal, including nine events with reconstructed energy in excess of 100 TeV, is clearly separated from the background.

Fitting the data to a superposition of extraterrestrial neutrinos on an atmospheric background yields a cosmic neutrino flux of

$$E_\nu^2 \frac{\mathrm{d}N}{\mathrm{d}E_\nu} = 3.6 \times 10^{-11}\,\mathrm{TeV\,cm^{-2}\,s^{-1}\,sr^{-1}} \tag{2.1}$$

for the sum of the three neutrino flavors. The energy and zenith angle dependence observed is consistent with what is expected for a flux of neutrinos produced by cosmic accelerators; see Fig. 4. The flavor composition of the flux is, after corrections for the acceptances of the detector to the different flavors, consistent with $\nu_e : \nu_\mu : \nu_\tau \sim 1 : 1 : 1$ as anticipated for a flux originating in cosmic sources.

The major uncertainty in the spectrum of atmospheric neutrinos at high energy is the flux of charm origin that must be present at some level. Short-lived charmed hadrons produced by cosmic rays in the atmosphere promptly decay, producing muons and neutrinos with the same spectrum as their parent cosmic rays. This “prompt" flux of leptons has not been identified. Existing limits [27, 28] allow a charm component at a level predicted by a dipole model calculation for the high-energy charm cross section [29]. In this context, it is important to point out that the muon produced in the same decay as the neutrino, in the case of muon neutrinos from above, is guaranteed to reach the detector provided that the neutrino energy is sufficiently high and the zenith angle sufficiently

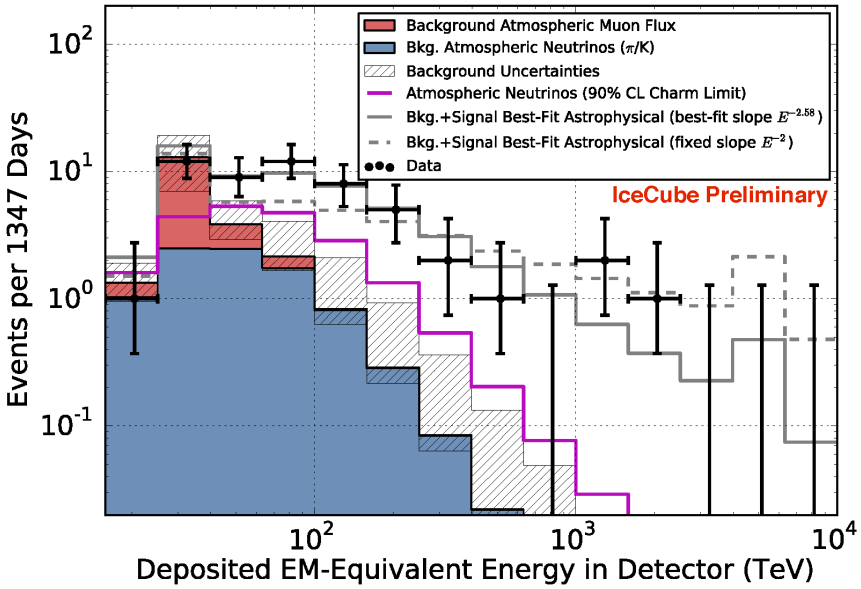

Figure 4: Deposited energies of muons observed in four years of data. The hashed region shows uncertainties on the sum of all backgrounds. The atmospheric muon flux (red) and its uncertainty is computed from simulation to overcome statistical limitations in our background measurement and scaled to match the total measured background rate. The atmospheric neutrino flux is derived from previous measurements of both the π, K and charm components of the atmospheric spectrum [26]. Also shown are two power-law fits to the spectrum.

small [30, 31]. In this case, the atmospheric neutrino provides its own self-veto. This self-veto is routinely applied to the IceCube data sample and suppresses any potential charm component.

In the meantime, two additional years of data have been analyzed, doubling the statistics of the discovery publication [32]. A purely atmospheric explanation can be excluded at 7σ. The four-year data set contains a total of 54 neutrino events with deposited energies ranging from 30 to 2000 TeV. In the fourth year, muon neutrinos were found that deposited ~ 500 TeV energy inside the detector, indicating PeV-energy parent neutrinos. One of them reconstructs through IceTop, IceCube's surface array, with no evidence for an air shower. Combining the absence of an air shower in IceTop with large deposited muon energy results in a high significance for astrophysical origin from a single event.

Recently, an independent analysis has also revealed an excess over atmospheric background of high-energy ν_μ-induced muons penetrating the Earth from the Northern Hemisphere [33, 34] confirming the signal observed in the starting event analyses; see Fig. 5, which shows the muon neutrino flux as a function of the energy deposited by the muons inside the detector. Standard Model physics allows one to infer the energy spectrum of the parent neutrinos; for instance, the highest energies in Fig. 5 correspond, on average, to parent neutrinos with energy in excess of PeV. A best fit to the spectrum that includes a conventional, charm and astrophysical component with free normalizations yields the results shown in the figure. With one additional year of data, the statistical significance exceeds $4.3\,\sigma$; in the 2014 sample, an event was found with energy 2.6 ± 0.3 PeV, representing the highest energy neutrino ever recorded, with energy in the $5 \sim 10$ PeV

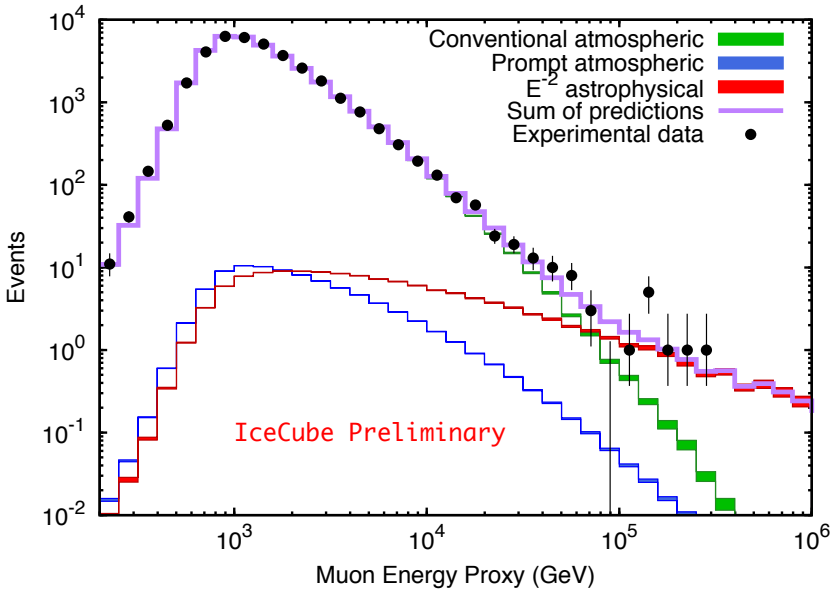

Figure 5: Spectrum of secondary muons initiated by muon neutrinos that have traversed the Earth, i.e., with zenith angle less than 5° above the horizon, as a function of the energy they deposit inside the detector. The highest energy muons are, on average, initiated by PeV neutrinos.

energy range [35].

Where do the cosmic neutrinos originate? Figure 6 shows the arrival directions of the four-year starting-event sample in Galactic coordinates. Cascade events are labeled (+), track events (×). The color scale indicates the value of the test statistic (TS) of an unbinned maximum likelihood test searching for anisotropies of the neutrino arrival directions. No significant local excess in the sky was found when compared to randomized pseudo-experiments. The correlation of neutrino events with the Galactic plane is not significant. Letting the width of the plane float freely, the best fit returned a correlation for a value of $\pm 7.5^\circ$ with a post-trial chance probability of 3.3%. Neither probability decreased after doubling the data. The IceCube Collaboration also searched for clustering of the events in time [36] and investigated a possible correlation with the times of observed GRBs [37]. No statistically significant correlation was found.

In summary, the observed neutrino flux is consistent with an isotropic distribution of arrival directions and equal contributions of all neutrino flavors [38], suggesting the observation of extragalactic sources whose flux has equilibrated in the three flavors after propagation over cosmic distances [39, 40]. Increasingly, a variety of analyses [38, 41] suggest that the cosmic neutrino flux dominates the atmospheric background above an energy that may be as low as 30 TeV with an energy spectrum that is not described as a single power. This is reinforced by the fact that fitting the excess flux in different ranges of energy yields different values for the power.

3. Closing in on the Sources

Rather than speculate, we will focus on the multimessenger connection of cosmic neutrinos to cosmic rays and gamma rays; this will turn out to be revealing. The overall energy density

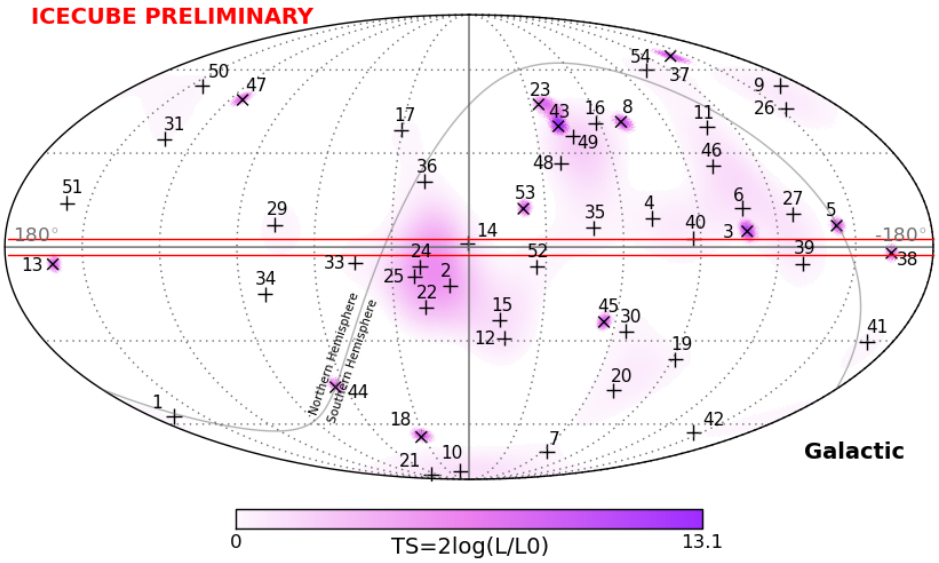

Figure 6: Arrival directions of neutrinos in the four-year starting-event sample in Galactic coordinates. Shower-like events are shown with "+" and those containing muon tracks with "×". The color scale indicates the value of the test statistic (TS) of an unbinned maximum likelihood test searching for anisotropies of the event arrival directions. The horizontal red lines indicate the minimum width (and step-size) $\pm 2.5^\circ$ used in the search for extended emission along the Galactic Plane. Note that the track-like event 28 has been omitted following the discussion in Ref. [32].

of the observed neutrino flux is close to the limit for neutrino production in the sources of ultra-high-energy (UHE) extragalactic CRs [42]. This may be a coincidence, but it may also indicate a multimessenger relation. The neutrino and CR nucleon (N) emission rates Q are related by

$$\frac{1}{3}\sum_\alpha E_\nu^2 Q_{\nu_\alpha}(E_\nu) \simeq \frac{1}{4}\frac{f_\pi K_\pi}{1+K_\pi} E_N^2 Q_N(E_N), \tag{3.1}$$

where $f_\pi (< 1)$ is the efficiency for pion production, K_π the ratio of charged to neutral pions, and $E_\nu \simeq 0.05 E_N$. The emission rate density of UHE CRs depends on their spectrum and composition, for a E^{-2} flux of protons $E_p^2 Q_p(E_p) \simeq (1-2)\times 10^{44}\,\mathrm{erg\,Mpc^{-3}\,yr^{-1}}$ [43]. Unlike cosmic rays that are collected from sources within the GZK radius of $\sim 100\,\mathrm{Mpc}$, neutrinos reach us from all redshifts. Their relative fluxes therefore depend on the evolution of the sources with redshift, which can be parametrized by a factor $\rho(z)$. For no evolution and $\gamma = 2$, $\xi_z \simeq 0.5$, whereas an evolution of sources following the star-formation rate (SFR) yields $\xi_z \simeq 2.4$. In the end, we obtain a diffuse neutrino flux given by

$$E_\nu^2 \phi_\nu(E_\nu) \simeq \frac{\xi_z f_\pi K_\pi}{1+K_\pi}(2-4)\times 10^{-8}\,\mathrm{GeV\,cm^{-2}\,s^{-1}\,sr}. \tag{3.2}$$

With $f_\pi < 1$ this reproduces the *Waxman-Bahcall* bound [42]. Interestingly, the observed flux is close to the bound requiring $f_\pi \simeq 1$ requiring a very efficient production of neutrinos in sources with optical thickness $\tau > 1$. These are often referred to as CR calorimeters or CR reservoirs [44], such as starburst galaxies [45, 46] and clusters of galaxies [47, 48, 49].

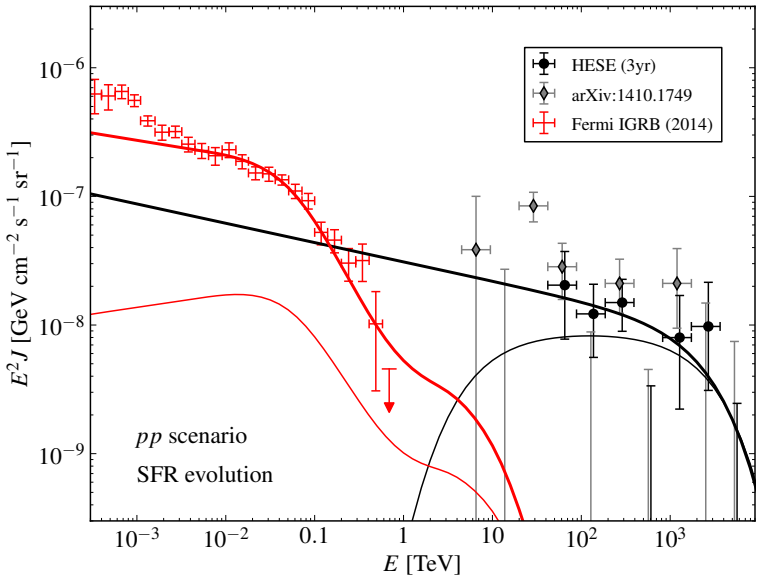

Figure 7: Two models of the astrophysical neutrino flux (black lines) observed by IceCube and the corresponding cascaded gamma-ray flux (red lines) observed by *Fermi*. The models assume that the decay products of neutral and charged pions from pp interactions are responsible for the nonthermal emission in the Universe [57]. The thin lines represent an attempt to minimize the contribution of the pionic gamma-ray flux to the *Fermi* observations. It assumes an injected flux of E^{-2} with exponential cutoff at low and high energy. The black data points are measured by the IceCube three-year "high-energy starting event" (HESE') analysis [32], the gray data points are from an IceCube analysis lowering the energy threshold for events starting in the detector even further [41].

The production of PeV neutrinos is inevitably associated with the production of PeV gamma rays [50, 51, 52, 53, 54, 55, 56]: hadronic accelerators produce fluxes of both neutral and charged pions that are the parents of gamma rays and neutrinos, respectively. The production rates of neutrinos and gamma rays are related by

$$\frac{1}{3}\sum_{\alpha} E_\nu^2 Q_{\nu_\alpha}(E_\nu) \simeq \frac{K_\pi}{4} E_\gamma^2 Q_\gamma(E_\gamma)\,. \tag{3.3}$$

Note that this relation does not depend on the pion production efficiency but only on the relative charged-to-neutral pion rate, K_π. On the other hand, the production rate of gamma rays described by Eq. (3.3) is not necessarily the emission rate observed. For instance, in hadronic sources that efficiently produce neutrinos via $p\gamma$ interactions, the target photon field can also efficiently reduce the pionic gamma rays via pair production. Also, inverse-Compton scattering and synchrotron emission in magnetic fields will shift the emitted gamma-ray spectrum to lower energies. This is a calorimetric process that will, however, conserve the total energy of hadronic gamma rays.

It is straightforward to apply the multimessenger relation to the cosmic neutrino flux observed by IceCube. Figure 7 shows the associated gamma-ray flux for two illustrative pp emission scenarios that accommodate the observed neutrino flux. The black and red lines show the neutrino and gamma-ray spectra after accounting for cosmic evolution and cascading in cosmic radiation

backgrounds. The thick solid line shows an $E^{-2.15}$ neutrino spectrum with an exponential cutoff around PeV. This scenario actually matches the extragalactic isotropic diffuse gamma-ray background (IGRB) measured by *Fermi* [58]. The alternative scenario illustrates that even for harder emission spectra the cascaded flux will still make a significant contribution to the Fermi IGRB. For illustration, we show the effect of hadronic emission that produces a peaked neutrino spectrum in the 10 TeV to 1 PeV energy region (thin black line). Note that such a spectrum is not expected for a pp scenario. The observed gamma-ray spectrum (thin red line) is in this case dominated by secondary cascaded photons. The contribution to the *Fermi* IGRB between 100 GeV to 1 TeV is still at the level of 10% even though the input neutrino spectrum underestimates the neutrino flux substantially. Soft emission spectra ($\Gamma \gtrsim 2.2$) are inconsistent with the Fermi observations [57, 59] and point at obscured or hidden sources.

In general, this exercise indicates that the diffuse gamma-ray contribution to the *Fermi* IGRB is large for pp cosmic beam dumps and suggests a common origin of some of the sources. This is intriguing because a recent analysis shows that blazars dominate the Fermi flux. Are blazars the final answer? The good news is that IceCube, by accumulating more events, can eventually identify blazars by observing multiple neutrinos from the same sources [60] . On the other hand, a search for neutrinos from *Fermi*'s *identified* blazars [61] has come up empty. However, these represent only 50% of the total diffuse background, allowing for the possibility that a partially different source population produces the neutrinos. Although no definite identification of the sources of cosmic neutrinos has emerged, it is rather clear that a multiwavelength path to the neutrino sources looks very promising.

By building IceCube, it was possible to map the optical properties of natural ice over large distances, and the IceCube Collaboration made the surprising discovery that the absorption length of the Cherenkov light to which the DOMs are sensitive exceeds 100 m. In fact, in the lower half of the detector it exceeds 200 m. The absorption length dictates the distance by which one can space the strings of sensors without spoiling the uniformity of the detector. Modeling indicates that spacings of 250 m, possibly larger, are acceptable. One can therefore instrument a ten-times-larger volume of ice with the same number of strings used to build IceCube. The project would be free of risk since the performance of the DOMs is well understood and we already know how to deploy them. Furthermore, the costs are also understood. Designed before 1999, all of the components of IceCube can be significantly updated for improved performance.

The larger spacings do of course result in a higher threshold, but this is not necessarily bad. While the 100,000 or so atmospheric neutrinos that IceCube collects above a threshold of 100 GeV every year were useful for calibration, they represent a severe background for isolating the cosmic component of the flux. The peak sensitivity to an E^{-2} spectrum is reached at 40 TeV [62]. While the detector has to be efficient below that energy, a threshold much lower than this value introduces background without a gain in signal. Designs for a next-generation instrument are in progress [63].

4. The Search for Dark Matter

IceCube was very much designed as a discovery instrument, and it covers a range of science, besides the search for the nature of the cosmic particle accelerators, whose interests are multidisciplinary. Examples includes the search for Galactic supernova explosions and the study of neutrinos

themselves, at higher energies and with improved statistics. Also, for some time now, neutrino "telescopes" have been recognized as powerful tools in the search for the particle nature of dark matter. IceCube's DeepCore infill, which lowers IceCube's threshold over a significant part of the detector volume, was initially proposed by Per Olof Hulth as a way to enhance IceCube's capabilities for detecting lower mass dark matter particles. In this context ,it is worth noting that the AMANDA detector, the forerunner and proof of concept for IceCube, received a significant fraction of its initial funding from the Berkeley Center for Particle Astrophysics to search for dark matter.

IceCube searches indirectly for dark matter by looking for neutrinos from concentrations of weakly interacting massive particles (WIMPs) in the Sun [64], in the Milky Way [65, 66], and in nearby galaxies [67]. The neutrinos are secondary products of annihilation of pairs of WIMPs into Standard Model particles, which include decays into neutrinos. The evidence that yet-to-be-detected weakly interacting massive particles (WIMPs) make up dark matter is compelling. WIMPs are swept up by the Sun as the Solar System moves about the galactic halo. Though interacting weakly, they will occasionally scatter elastically with nuclei in the Sun and lose enough momentum to become gravitationally bound. Over the lifetime of the Sun, a sufficient density of WIMPs may accumulate in its center so that an equilibrium is established between their capture and annihilation. The annihilation products of these WIMPs represent an indirect signature of halo dark matter, their presence revealed by neutrinos that escape the Sun with minimal absorption. The neutrinos are, for instance, the decay products of heavy quarks and weak bosons resulting from the annihilation of WIMPs into $\chi\chi \rightarrow \tau\bar{\tau}$, $b\bar{b}$ or W^+W^-. Neutrino telescopes have are sensitive to such neutrinos because of the relatively large neutrino energy reflecting the mass of the WIMP.

The beauty of the indirect detection technique using neutrinos originating in the Sun is that the astrophysics of the problem is understood. The source in the Sun has built up over solar time, sampling the dark matter throughout the galaxy; therefore, any possible structure in the halo has been averaged out. Given a WIMP mass and properties, one can unambiguously predict the signal in a neutrino telescope. If not observed, the model is ruled out. This is in contrast to indirect searches for photons from WIMP annihilation, whose sensitivity depends critically on the structure of halo dark matter; observation requires cuspy structure near the galactic center or clustering on appropriate scales elsewhere. Observation not only necessitates appropriate WIMP properties but also favorable astrophysical circumstances.

Extensions of the Standard Model of quarks and leptons, required to solve the hierarchy problem, naturally yield dark matter candidates. For instance, the neutralino, the lightest stable particle in supersymmetric models, has been intensively studied as a possible dark matter candidate. Detecting it has become the benchmark by which experiments are evaluated and mutually compared. We will follow this tradition here. Supersymmetric models allow for a large number of free parameters and, unfortunately, for a variety of parameter sets that are able to generate the observed dark matter density in the context of standard big bang cosmology. The neutralino interacts with ordinary matter by spin-independent (e.g., Higgs exchange) and by spin-dependent (e.g., Z-boson exchange) interactions. The first mechanism favors direct detection experiments [68] because the WIMP interacts coherently, resulting in an increase in sensitivity proportional to the square of the atomic number of the detector material. Given the rapid improvement in the sensitivity of direct experiments, indirect detection experiments are therefore not competitive for models in which dark

matter has a large spin-independent coupling. We will show that this is not the case for spin-dependent models, however. Within the context of supersymmetry, direct and indirect experiments are complementary.

Although IceCube detects neutrinos of all flavors, sensitivity to neutrinos produced by WIMPs in the Sun is achieved by exploiting the degree accuracy with which muon neutrinos can be pointed back to the Sun.

IceCube is most sensitive to WIMPs with significant spin-dependent cross sections for interactions with protons because this would lead to strong concentrations in the Sun, a nearby and readily identifiable source. The signal would simply be an excess of neutrinos of GeV energy and above from the direction of the Sun over the atmospheric neutrino background in the same angular window. There would be no alternative astrophysical explanation of such a signal, which represents a smoking gun for dark matter particles. In most WIMP scenarios, the cross sections for WIMP capture ($\sigma_{\chi,p}$) and for WIMP annihilation ($\sigma_{\chi,\chi}$) are large enough so that an equilibrium between capture and annihilation would have been achieved within the age of the solar system [69]. In this case, limits on neutrinos from the Sun can be expressed in terms of the capture cross section, $\sigma_{\chi,p}$. If equilibrium is not reached, weaker limits can still be derived.

A WIMP may interact with ordinary nuclei by spin-independent (e.g. Higgs exchange) and by spin-dependent (e.g. Z-boson exchange) interactions. The first mechanism favors direct detection experiments [68] because the WIMP interacts coherently, resulting in an increase in sensitivity proportional to the square of the atomic number of the detector material. The latter favors indirect experiments in which the rates are dominated by spin-dependent interactions with protons. In the case of the Sun, the WIMPS have accumulated over solar time scales, sampling the dark matter throughout the galaxy and averaging out any structure in the halo that theory may not have accounted for. Within the context of supersymmetry, direct and indirect experiments are complementary.

Quantitative interpretation of the IceCube limits is complicated, depending on detailed analysis of capture rates and annihilation channels. The analysis uses DarkSUSY [69], which builds on the classic calculations of Gould [70] for capture and annihilation rates. The neutrino spectrum from annihilation of pairs of WIMPs depends on the dominant channel for coupling to Standard Model particles. The neutrino spectrum at production is also modified by subsequent interactions and oscillations of neutrinos as they propagate out from the solar core. Three flavor oscillations with matter effects are included, as in Ref. [71]. The range of possibilities is bracketed by calculating two extremes,

$$\chi\,\chi \to b\bar{b}\,(\text{soft}) \text{ and } \chi\,\chi \to W^+W^-,\ \tau\bar{\tau}\,(\text{hard}). \tag{4.1}$$

In the hard channel, $W^\pm$ are replaced by $\tau^\pm$ for $m_\chi < m_W$.

The current IceCube limits [64, 72, 73] are shown in Figs. 8 and 9. Also shown is a sampling of the WIMP parameter space that is not ruled out by other experiments. IceCube has produced the most stringent limits on the cross section for spin-dependent interactions of dark matter particles with ordinary matter. Since the exact branching ratios of WIMP annihilation into different channels is model-dependent, experiments usually choose two annihilation channels which give extreme neutrino spectra to show their results. Annihilation into $b\bar{b}$ is chosen as a representative case producing a soft neutrino spectrum, and annihilation into W^+W^- or $\tau\bar{\tau}$ as a hard spectrum.

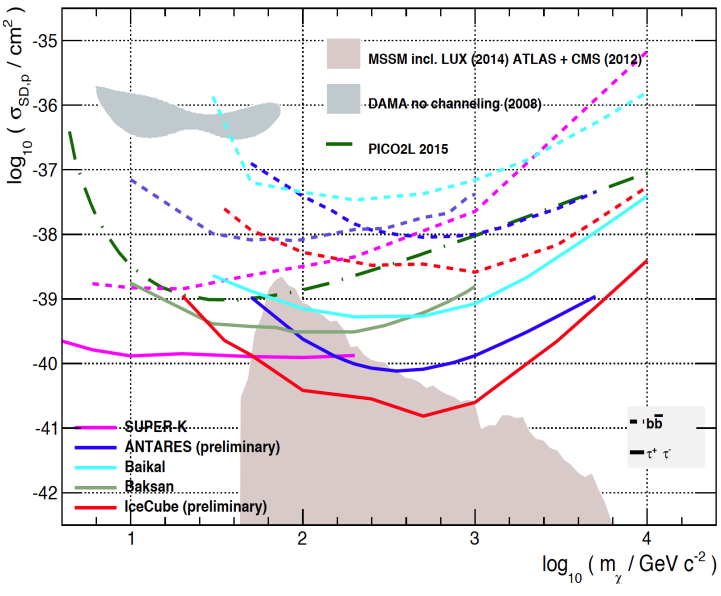

Figure 8: Upper limits at 90% confidence level on the spin-dependent neutralino-proton cross section assuming that the neutrinos are produced by $b\bar{b}$, $\tau\bar{\tau}$ and W^+W^- annihilation. Limits from IceCube [64, 72, 73], Super-K [75], ANTARES [76], Baikal [77] and Baksan [78] are shown. Full lines refer to limits on the annihilation channel and dashed lines to the $b\bar{b}$ channel. Direct search results from PICO [79] and LUX [80] and tentative signal regions [81, 82, 83] (gray-shaded areas) are included for comparison. The brown-shaded region indicates the allowed parameter space in the MSSM not ruled out by direct experiments.

Assuming a 100% branching ratio to each of these channels brackets the expected neutrino spectrum from any more realistic model with branching to more channels. IceCube or SuperK reach bounds at the $10^{-40} - 10^{-41}\text{cm}^2$ level, covering the WIMP mass range, between the two experiments, from a few GeV to 100 TeV. Because of the A^2 coherence factor for scattering on heavy nuclei, the indirect experiments have an advantage over IceCube for the case of spin-independent interactions; see Fig. 9.

Current IceCube limits are based on observations of ν_μ-induced muons with the nearly complete detector, with 79 strings of digital optical modules (DOMs) and including for the first time the DeepCore subarray. Data were collected from May 2010 to May 2011, including the austral summer (October-March) when the Sun is above the horizon. By including events that start inside DeepCore (summer and winter), the mass range for the WIMP search could be extended down to 20 GeV, which overlaps some of the allowed region from the DAMA experiment [74]. By including muons from below the horizon entering IceCube from outside (winter only because of the high background of cosmic-ray muons from above), the mass range is extended to 5 TeV.

Note that the limits are derived from a single year of data with a detector that was not quite completed. Not only are the analysis methods subject to improvements, five years of data is now available and will be analysed in the near future. This will yield a discovery or limits improved well beyond the square root of time expected from statistics alone.

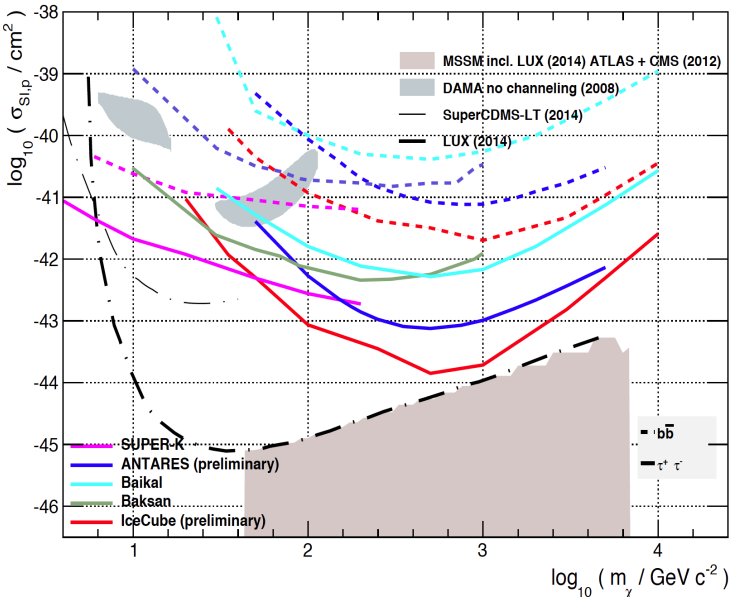

Figure 9: Same as the previous figure for spin-independent interactions of dark matter with ordinary matter.

References

[1] F. Reines and C. L. Cowan 1956 *Nature* **178** 446–449

[2] K. Greisen 1960 *Ann.Rev.Nucl.Part.Sci.* **10** 63–108

[3] F. Reines 1960 *Ann.Rev.Nucl.Part.Sci.* **10** 1–26

[4] M. Markov 1960 *Proc. of the 10th Intl. Conf. on High-Energy Physics* 578–581

[5] T. K. Gaisser, F. Halzen and T. Stanev 1995 *Phys.Rept.* **258** 173–236 [hep-ph/9410384]

[6] J. Learned and K. Mannheim 2000 *Ann.Rev.Nucl.Part.Sci.* **50** 679–749

[7] F. Halzen and D. Hooper 2002 *Rept.Prog.Phys.* **65** 1025–1078 [astro-ph/0204527]

[8] J. K. Becker 2008 *J.Phys.Conf.Ser.* **136** 022055 [0811.0696]

[9] A. Roberts 1992 *Rev.Mod.Phys.* **64** 259–312

[10] V. Berezinsky and G. Zatsepin 1969 *Phys.Lett.* **B28** 423–424

[11] Zheleznykh, I., Int. J. Mod. Phys. A 21S1 (2006) 1; Markov, M. and Zheleznykh, I., Nucl. Phys. 27 (1961) 385

[12] J. Babson *et al.* (DUMAND Collaboration) 1990 *Phys.Rev.* **D42** 3613–3620

[13] V. Balkanov *et al.* (BAIKAL collaboration) 2003 *Nucl.Phys.Proc.Suppl.* **118** 363–370

[14] G. Aggouras *et al.* (NESTOR Collaboration) 2005 *Astropart.Phys.* **23** 377–392

[15] J. Aguilar *et al.* (ANTARES Collaboration) 2006 *Astropart.Phys.* **26** 314–324 [astro-ph/0606229]

[16] E. Migneco 2008 *J.Phys.Conf.Ser.* **136** 022048

[17] A. Margiotta (KM3NeT) 2014 *JINST* **9** C04020 [1408.1132]

[18] P. Bagley *et al.* 2001 *IceCube Preliminary Design Document* (The IceCube Collaboration) http://www.icecube.wisc.edu/science/publications/pdd/pdd.pdf

[19] J. Ahrens *et al.* (IceCube Collaboration) 2004 *Astropart.Phys.* **20** 507–532 [astro-ph/0305196]

[20] F. Halzen and S. R. Klein 2010 *Rev. Sci. Instrum.* **81** 081101 [1007.1247]

[21] F. Halzen 2013 *Riv.Nuovo Cim.* **36** 81–104

[22] M. Aartsen *et al.* (IceCube Collaboration) 2013 *Nucl.Instrum.Meth.* **A711** 73–89 [1301.5361]

[23] J. Ahrens *et al.* (AMANDA Collaboration) 2004 *Nucl.Instrum.Meth.* **A524** 169–194 [astro-ph/0407044]

[24] M. Aartsen *et al.* (IceCube Collaboration) 2014 *JINST* **9** P03009 [1311.4767]

[25] M. Aartsen *et al.* (IceCube Collaboration) 2013 *Phys.Rev.Lett.* **111** 021103 [1304.5356]

[26] M. Aartsen *et al.* (IceCube Collaboration) 2014 *Phys.Rev.* **D89** 102001 [1312.0104]

[27] M. Aglietta *et al.* (LVD Collaboration) 1999 *Phys.Rev.* **D60** 112001 [hep-ex/9906021]

[28] A. Schukraft (IceCube Collaboration) 2013 *Nucl.Phys.Proc.Suppl.* **237-238** 266–268 [1302.0127]

[29] R. Enberg, M. H. Reno and I. Sarcevic 2008 *Phys.Rev.* **D78** 043005 [0806.0418]

[30] S. Schönert, T. K. Gaisser, E. Resconi and O. Schulz 2009 *Phys.Rev.* **D79** 043009 [0812.4308]

[31] T. K. Gaisser, K. Jero, A. Karle and J. van Santen 2014 *Phys.Rev.* **D90** 023009 [1405.0525]

[32] M. Aartsen *et al.* (IceCube Collaboration) 2014 *Phys.Rev.Lett.* **113** 101101 [1405.5303]

[33] M. G. Aartsen *et al.* (IceCube) 2015 *Phys. Rev. Lett.* **115** 081102 [1507.04005]

[34] C. Weaver 2014 Spring APS Meeting, Savannah, Georgia, USA

[35] S. Schoenen and L. Rädel 2015 *Proceedings of ICRC2015* **1079** 642

[36] M. G. Aartsen *et al.* (IceCube) 2015 *Astrophys. J.* **807** 46 [1503.00598]

[37] M. G. Aartsen *et al.* (IceCube) 2015 *Astrophys. J.* **805** L5 [1412.6510]

[38] M. Aartsen *et al.* (IceCube Collaboration) 2015 [1502.03376]

[39] J. G. Learned and S. Pakvasa 1995 *Astropart.Phys.* **3** 267–274 [hep-ph/9405296]

[40] H. Athar, M. Jezabek and O. Yasuda 2000 *Phys.Rev.* **D62** 103007 [hep-ph/0005104]

[41] M. Aartsen *et al.* (IceCube Collaboration) 2014 [1410.1749]

[42] E. Waxman and J. N. Bahcall 1999 *Phys.Rev.* **D59** 023002 [hep-ph/9807282]

[43] M. Ahlers and F. Halzen 2012 *Phys.Rev.* **D86** 083010 [1208.4181]

[44] B. Katz, E. Waxman, T. Thompson and A. Loeb 2013 [1311.0287]

[45] A. Loeb and E. Waxman 2006 *JCAP* **0605** 003 [astro-ph/0601695]

[46] I. Tamborra, S. Ando and K. Murase 2014 *JCAP* **1409** 043 [1404.1189]

[47] V. Berezinsky, P. Blasi and V. Ptuskin 1997 *Astrophys J.* **487** 529–535 [astro-ph/9609048]

[48] K. Murase, S. Inoue and S. Nagataki 2008 *Astrophys.J.* **689** L105 [0805.0104]

[49] F. Zandanel, I. Tamborra, S. Gabici and S. Ando 2014 [1410.8697]

[50] J. Alvarez-Muniz and F. Halzen 2002 *Astrophys.J.* **576** L33–L36 [astro-ph/0205408]

[51] D. Fox, K. Kashiyama and P. Meszaros 2013 *Astrophys.J.* **774** 74 [1305.6606]

[52] M. Gonzalez-Garcia, F. Halzen and V. Niro 2014 *Astropart.Phys.* **57-58** 39–48 [1310.7194]

[53] T. K. Gaisser 2013 *EPJ Web Conf.* **53** 01012

[54] P. Padovani and E. Resconi 2014 *Mon.Not.Roy.Astron.Soc.* **443** 474–484 [1406.0376]

[55] L. A. Anchordoqui, H. Goldberg, T. C. Paul, L. H. M. da Silva and B. J. Vlcek 2014 [1410.0348]

[56] A. M. Brown, J. Adams and P. M. Chadwick 2015 [1505.00935]

[57] K. Murase, M. Ahlers and B. C. Lacki 2013 *Phys.Rev.* **D88** 121301 [1306.3417]

[58] M. Ackermann *et al.* (The Fermi LAT collaboration) 2014 [1410.3696]

[59] X.-C. Chang and X.-Y. Wang 2014 *Astrophys.J.* **793** 131 [1406.1099]

[60] M. Ahlers and F. Halzen 2014 [1406.2160]

[61] T. Glüsenkamp (IceCube) 2015 [1502.03104]

[62] F. Halzen, A. Kappes and A. O'Murchadha 2008 *Phys.Rev.* **D78** 063004 [0803.0314]

[63] M. Aartsen *et al.* (IceCube Collaboration) 2014 [1412.5106]

[64] M. Aartsen *et al.* (IceCube collaboration) 2013 *Phys.Rev.Lett.* **110** 131302 [1212.4097]

[65] R. Abbasi *et al.* (IceCube Collaboration) 2011 *Phys.Rev.* **D84** 022004 [1101.3349]

[66] R. Abbasi *et al.* (IceCube) 2012 [1210.3557]

[67] M. Aartsen *et al.* (IceCube Collaboration) 2013 *Phys.Rev.* **D88** 122001 [1307.3473]

[68] B. Sadoulet 2007 *Science* **315** 61

[69] P. Gondolo, J. Edsjo, P. Ullio, L. Bergstrom, M. Schelke and E. A. Baltz 2004 *JCAP* **0407** 008 [astro-ph/0406204]

[70] A. Gould 1992 *Astrophys. J.* **388** 338–344

[71] M. Blennow, J. Edsjo and T. Ohlsson 2008 *JCAP* **0801** 021 [0709.3898]

[72] M. G. A. et al. 2015 *PoS* **ICRC2015**

[73] M. G. A. et al. 2015 *PoS* **ICRC2015**

[74] P. Ullio, M. Kamionkowski and P. Vogel 2001 *JHEP* **07** 044 [hep-ph/0010036]

[75] K. Choi *et al.* (Super-Kamiokande) 2015 *Phys. Rev. Lett.* **114** 141301 [1503.04858]

[76] C. T. et al. 2015 *PoS* **ICRC2015**

[77] A. D. Avrorin *et al.* (Baikal) 2014 *Astropart. Phys.* **62** 12–20 [1405.3551]

[78] M. M. Boliev, S. V. Demidov, S. P. Mikheyev and O. V. Suvorova 2013 *JCAP* **1309** 019 [1301.1138]

[79] C. Amole *et al.* (PICO) 2015 *Phys. Rev. Lett.* **114** 231302 [1503.00008]

[80] D. S. Akerib *et al.* (LUX) 2014 *Phys. Rev. Lett.* **112** 091303 [1310.8214]

[81] C. Savage, G. Gelmini, P. Gondolo and K. Freese 2009 *JCAP* **0904** 010 [0808.3607]

[82] C. E. Aalseth *et al.* 2011 *Phys. Rev. Lett.* **107** 141301 [1106.0650]

[83] R. Agnese *et al.* (CDMS) 2013 *Phys. Rev. Lett.* **111** 251301 [1304.4279]